A Letters Journal Exploring the Frontiers of Physics

February 2020

EPL, **129** (2020) 37001 www.epljournal.org
doi: 10.1209/0295-5075/129/37001

Regulating the electronic and optic properties of hexagonal boron nitride nanosheets via phosphorus doping

Jing Zhang[1,2], Bin Zhang[2,3], Yuanlie Yu[2,3(a)] and Chun-Ming Wang[1,4(b)]

[1] *School of Physics, State Key Laboratory of Crystal Materials, Shandong University - Jinan Shandong 250100, PRC*
[2] *R&D Center of Lubricating and Protecting Materials, Lanzhou Institute of Chemical Physics, Chinese Academy of Sciences - Lanzhou 730000, PRC*
[3] *Center of Materials Science and Optoelectronics Engineering, University of Chinese Academy of Sciences Beijing 100049, PRC*
[4] *Center for Optics Research and Engineering (CORE), Key Laboratory of Laser and Infrared System of Ministry of Education, Shandong University - Qingdao, Shandong 266237, PRC*

received 9 December 2019; accepted in final form 10 February 2020
published online 26 February 2020

PACS 73.20.At – Surface states, band structure, electron density of states
PACS 74.25.Gz – Optical properties
PACS 31.15.E- – Density-functional theory

Abstract – The application of hexagonal boron nitride nanosheets (*h*-BNNSs) in electronical and optical fields is limited due to their wide band gap. In this letter, we report a first-principles study on the electronic and optic properties of phosphorus (P) functionalized *h*-BNNSs. The results show that the introduction of P atoms leads to a valid modification of *h*-BNNS band structure which can reduce the width of band gap from 4.643 eV to 0.824 eV. The transformation from insulator to semiconductor of h-BNNSs is achieved through this band width regulation, and all P-doped *h*-BNNSs exhibit an active response to the visible light. In particular, with the increase in the number of doped P atoms, the absorption wavelength range can cover the whole visible region. In terms of the analysis of electronic structures and absorption spectra of the P-doped *h*-BNNSs, an enhancement mechanism of the visible-light response for the effect of the introduction of P atoms is proposed. It is expected that P-doped *h*-BNNSs could be used as potential metal-free efficient visible-light–driven photocatalysts.

Introduction. – Hexagonal boron nitride nanosheets (*h*-BNNSs) are one of the leading constituents in the field of two-dimensional (2D) material research due to their excellent chemical and physical properties, such as good chemical inertness, high oxidation resistance and outstanding electrical insulation [1–3]. These unique properties make *h*-BNNSs very attractive in wide applications including lubrication, fire resistance, corrosion resistance, etc. [4–7]. However, the large band gap of pure *h*-BNNSs which is about 6.0 eV greatly restricts their application as semiconductor and optical devices [8], since this wide band gap confines the *h*-BNNSs within insulation and deep ultraviolet absorption range. Previous theoretical [9–13] and experimental [14,15] works have demonstrated that chemical modification of *h*-BNNSs with various dopants, such as fluorine (F), hydrogen (H), and oxygen (O), can effectively tune the band gap of *h*-BNNSs, providing a promising approach to engineer the band gap of *h*-BNNSs for different applications. Hydrogenation and fluorination of *h*-BNNSs will lead to a reduction in the band gap of the sheets, thus making the system possess new electrical, magnetic and optical characteristics. For example, the fluorination of BN nanotubes will result in highly curled tubular BN sheets and make insulating BN nanotubes become semi-conductive [16–20], and semi-hydrogenated graphitic BN sheet can be used as a potential metal-free visible-light–driven photo-catalyst for water splitting [12]. Moreover, the band gap of *h*-BNNSs can be further narrowed to about 1.7 eV through oxygen doping and/or functionalization [14]. These obtained oxygen doped h-BNNSs exhibit strong absorptions within the whole ultra-violet (UV) (<400 nm), violet and blue light ranges, and show the absorption onset at about

(a) E-mail: yuanliehll@licp.cas.cn
(b) E-mail: wangcm@sdu.edu.cn

Table 1: Summaries of the lattice parameters, the cohesive energies, Fermi level, band gaps, VBM and CBM for six different P-doped h-BNNSs and h-BN.

Systems	Lattice parameters (Å)	E_{coh} (eV/atom)	Fermi level (eV)	Band gap (eV)	VBM (eV)	CBM (eV)
h-BN	$a = b = 10.016$, $c = 20.000$	7.02	−4.179	4.643	−6.019	−1.375
P1-h-BN	$a = b = 10.256$, $c = 16.499$	6.79	−3.579	3.595	−5.350	−1.755
P3-h-BN	$a = b = 10.524$, $c = 16.754$	6.41	−3.654	2.853	−5.029	−2.176
P5-h-BN	$a = 11.047$, $b = 10.988$, $c = 18.001$	6.01	−4.018	2.529	−5.273	−2.745
P7-h-BN	$a = b = 11.298$, $c = 19.477$	5.76	−4.069	1.864	−4.943	−3.079
P9-h-BN	$a = 11.566$, $b = 11.446$, $c = 18.185$	5.50	−4.322	1.744	−5.181	−3.437
P16-h-BP	$a = b = 12.119$, $c = 20.304$	4.80	−4.526	0.824	−4.928	−4.104

800 nm [14]. In our previous work, the F-doped h-BNNSs with 37.5 at.% and 50 at.% doping ratios also achieved the absorption of visible light [21].

However, regulation of the electronic and optic properties of h-BNNSs by surface functionalization will cause h-BNNSs to form bending deformation or produce magnetism, thus influencing the unique properties of h-BNNSs. Therefore, it is necessary to modify the electronic and optic properties of h-BNNSs while maintaining their planarity and nonmagnetism. Phosphorus (P) and N atoms have the same valence electronic configuration, so the substitution of P with an N atom would not lead to the structure change of the h-BNNSs. There is little previous research work on the P-doped h-BNNSs. The main research is that a single P-doped h-BNNS can achieve visible light absorption [22], but the effect on the electrical properties of h-BNNS and its relationship with content are discussed to be almost none. In terms of the above analysis, P atoms are selected to substitute N atoms in h-BNNSs to regulate the electronic and optic properties and the relationship between them and the number of P atoms of h-BNNSs.

Herein, the P-doped h-BNNSs with different P atoms have been designed to investigate the electronic and optic properties of P-doped h-BNNSs using density functional theory (DFT) based on the first-principles calculations. The band structure, partial density of states (PDOS), optical absorption spectra and imaginary part of the dielectric function were calculated and analysed. Finally, based on the analysis of the electronic structure and absorption spectrum, an enhanced mechanism of the visible light absorption was proposed. The better electronic and optic properties of P-doped h-BNNSs make them promising 2D semiconductor materials and visible-light active photocatalysts.

Method. – The calculated structures, electronic and optic properties are determined on the basis of first-principles density functional theory (DFT) implemented in the CASTEP modules of Material Studio [23,24]. The electronics interactions were described using a norm-conserving pseudopotential serving as the plane wave base [25]. The Perdew-Burke-Ernzerh (PBE) generalized gradient approximation (GGA) [26] with long-range dispersion correction via Grimme's scheme [27] was used to approximate the exchange-correlation potential. The energy cut-off and the real-space global cut-off radius were set to 540 eV and 4.1 Å for all these calculations, respectively. A convergence criterion, which is 1.0×10^{-5} eV/atom for energy, 0.03 eV/Å for maximum force and 0.001 Å for maximum displacement on every atom, was performed to optimize the geometry structure. In order to model P-doped h-BNNSs, a larger super-cell ($4\times4\times1$) was repeated periodically on the x-y plane. A vacuum space was set to be 20 Å to avoid the interaction between adjacent layers. After the convergence test, the Brillouin zone was sampled by $12 \times 12 \times 1$ k-points using the Monkhorst-Pack (MP) scheme [28] to carry out the calculations of the electronic and optic properties. The whole calculated values were obtained at 0 K.

Results and discussion. – Before addressing the electronic and optic properties of P-doped h-BNNSs, the primitive h-BNNS is revisited in order to use its electronic properties as a frame of reference. Table 1 lists the cohesive energy, lattice and band structure parameters of the primitive and also of the P-doped h-BNNSs. The band structure is non-spin-polarized and exhibits a direct bandgap of 4.643 eV. Due to the large band gap, the pristine h-BNNS is a direct band gap insulator (fig. 1(b)). The Fermi level is near the top of the valence band (VB). For the pristine h-BNNS, the valence band maximum (VBM) and conduction band minimum (CBM) are due to the p electrons of N and B atoms, respectively (fig. 1(c)). The electrons are accumulated between the covalent B-N bonds and shared by the hexatomic ring composed by B and N atoms, showing a typical conjugated π bond (fig. 1(d)).

In order to study the effect of P atoms on the geometric structure, we have investigated the stable structure of the different numbers of P doping h-BNNSs, as shown in fig. 2.

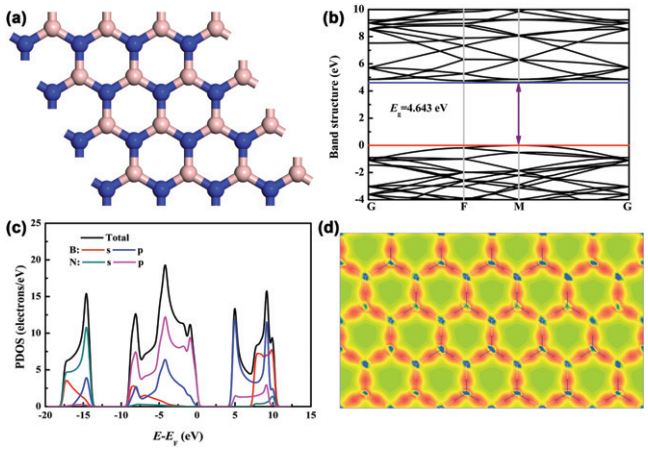

Fig. 1: Structure and electrical properties of h-BN. (a) the structure optimization diagram, (b) the band structure, (c) the PDOS, and (d) the 2D deformation electron density. Pink balls represent B atoms and blue balls represent N atoms.

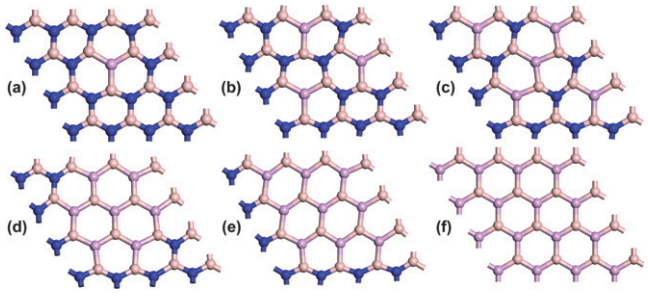

Fig. 2: The structure optimization diagram for the P-doped h-BNNSs with different P atoms: (a) P1-h-BN, (b) P3-h-BN, (c) P5-h-BN, (d) P7-h-BN, (e) P9-h-BN, and (f) h-BP. Pink, blue, and purple balls represent B, N, and P atoms, respectively.

As we all know, the electronegativity of P atoms (2.1) is smaller than that of N atoms (3.0) while the atomic radius of P is larger than that of N atoms, so the bond lengths and bond angles of the surface structure will change, causing deformation of the original hexagonal structure and broadening the lattice parameters of P doping h-BNNSs. Fully P-doped nanosheets, known as h-BPNSs, also have regular hexagonal structures, but the corresponding bond lengths and surfaces are elongated. The detail crystal constants are shown in table 1. The decrease of the electronegativity of P atoms reduces the structural stability of the system. Nevertheless, the intrinsic structure stability of the 2D materials is one of the most important factors influencing the successful applications. Therefore, it is necessary to determine the binding properties of the atoms in the P-doped h-BNNSs. The cohesive energy which is the energy required to decompose the doped h-BNNSs into isolated B, N and P atoms can be used to represent the stability. Here the cohesive energy was estimated using the following equation:

$$E_{\rm coh} = (nE_{\rm B} + mE_{\rm N} + pE_{\rm P} - E_{\rm total})/(n+m+p), \quad (1)$$

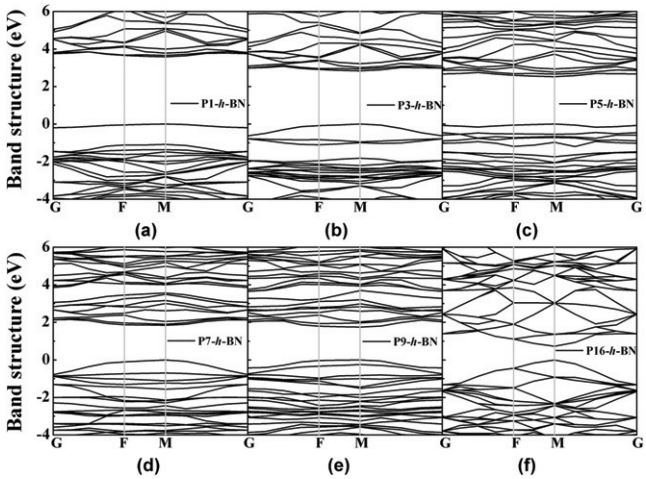

Fig. 3: The band structure for the P-doped h-BNNSs with different P atoms: (a) P1-h-BN, (b) P3-h-BN, (c) P5-h-BN, (d) P7-h-BN, (e) P9-h-BN, and (f) h-BP.

where $E_{\rm B}$, $E_{\rm N}$, $E_{\rm P}$, and $E_{\rm total}$ are the energies of single B atom, single N atom, single P atom, and a doped h-BNNS supercell, respectively. n, m, and p are the number of B, N and P atoms of a doped h-BNNS supercell, respectively. The values of the cohesive energies for different numbers of P-doped h-BNNSs are shown in table 1. With the increase of the number of P atoms, the cohesive energy of the system decreases. The cohesive energy of partial P substitution is higher than those of MoS_2 (5.18–5.44 eV/atom) [29,30] and silicene (3.49 eV/atom) [31], but lower than those of pure h-BNNSs (7.01 eV/atom) [32] and graphene (7.62 eV/atom) [31]. This shows that compared with MoS_2 and silicene, the P-doped h-BNNSs have better structure stability.

It is well known that the electronic and optic properties are strongly related to the electronic structures. To study the P doping effect on the electronic structures, the band structure and density of states (DOS) are calculated and illustrated in figs. 3–5, respectively. As a whole, like the pristine h-BNNSs, all the P-doped h-BNNSs still have a direct band gap at the M point. The direct band gap is more favourable for light absorption. However, with the increase of the number of P atoms in the P-doped h-BNNSs, the width of the band gap gradually becomes narrow, which is in the range from 3.595 eV to 0.824 eV. This shows that the P doping can make h-BNNSs become semiconductors. This change is attributed to the redistribution of the DOSs caused by P doping. Figure 4 shows the variation of the band gaps, VBMs and CBMs of the P-doped h-BNNSs as a function of numbers of P atoms. The reduction of the band gap of P-doped h-BNNSs is related to the rapid decline of CBM and the slow rise of VBM (fig. 4). All CBMs shift downward to the Fermi level (table 1), indicating a P-type doping. The downward of the CBM is mainly due to the fact that the bottom of the CB is controlled by the B 2p electrons. After doping with

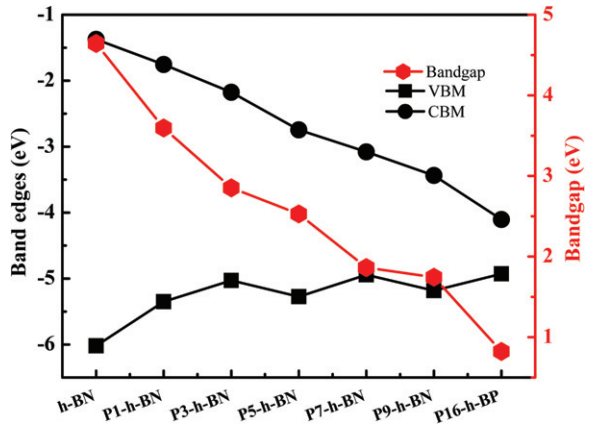

Fig. 4: Change in band gap, VBM and CBM as a function of the numbers of P-doped atoms calculated from DFT calculations.

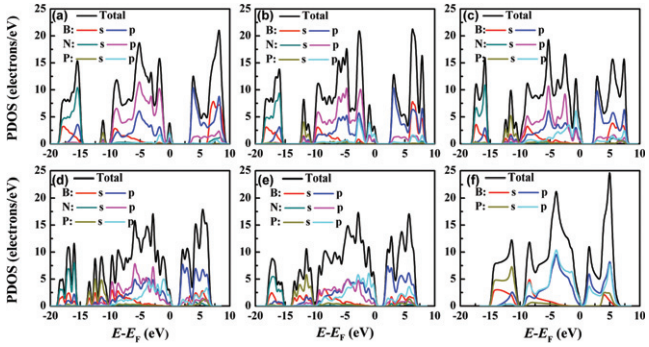

Fig. 5: The partial density of states (PDOS) for the P-doped *h*-BNNSs with different P atoms: (a) P1-*h*-BN, (b) P3-*h*-BN, (c) P5-*h*-BN, (d) P7-*h*-BN, (e) P9-*h*-BN, and (f) *h*-BP.

P atoms, because the P 3*p* state has lower energy than the N 2*p* state, the B 2*p* state electrons can form lower energy antibonding with the P 3*p* state electrons, thus forming a lower CB. Thus, the CBM moves down due to the low electron energy in the P 3*p* state. The VBM below the Fermi level is mainly constructed by P 3*p* orbitals, and B 2*p* contributes significantly to the CBM, which means the most possible electron transition occurs from P 3*p* to B 2*p* within the band gap. For P1 and P3-doped *h*-BNNSs, two intermediate bands (IB) appear evidently close to the Fermi level, which are P 3*p* at the Fermi level and another P 3*p* and N 2*p* at −0.9 eV (fig. 5(a) and (b)). Due to the appearance of IB, the band gap from VBM to CBM is reduced. Under these circumstances, a two-step electron transition path emerges from VBM to CBM, that is to say, the electron first transits from N 2*p* at VBM to IB and then from IB to B 2*p* at CBM. As the number of P-doped atoms increases, the IB energy level enters into the original VBM level and forms a new VBM level (figs. 5(c)–(f)). It also has an important effect on reducing the band gap width. Remarkably, based on the above descriptions, it makes the electron transition much easier under excitation. Therefore, it is predicted that the absorption range of light can be extended. Furthermore,

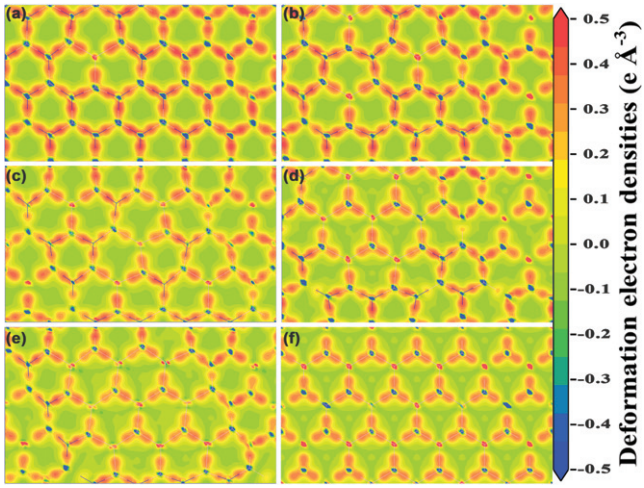

Fig. 6: The 2D deformation electron densities (in units of e $Å^{-3}$) maps for the P-doped h-BNNSs with different numbers of P atoms: (a) P1-*h*-BN, (b) P3-*h*-BN, (c) P5-*h*-BN, (d) P7-*h*-BN, (e) P9-*h*-BN, and (f) *h*-BP. The red area represents electron accumulation and blue area refers to electron depletion.

fig. 5 also shows that a strong hybridization between B 2*p* and P 2*p* is observed which indicates the formation of a strong covalent chemical bond between them. This phenomenon further demonstrates that the P-doped system has good structural stability. The difference between the values of DOS of the P and N atoms indicates that the electronegativity of P (2.1) is lower than that of N (3.0) atoms. Almost the same DOS is consistent with the approximate electronegativity of the B (2.0) and P atoms.

To study the electron redistribution induced by the effect of P atoms, the 2D deformation electron density maps are illustrated in fig. 6. As we all known, for the pure *h*-BNNS, the electrons are accumulated between the covalent B-N bonds and shared by the hexatomic ring composed by N and B atoms, showing a typical conjugated π bond (fig. 1(d)). After the introduction of P atoms, the electron distributions localized around the doping area have been varied (fig. 6). P atoms have weakened the conjugated π bonding between the P atoms and the adjacent B atoms. This weakening and breaking are mainly due to the increment of bond ionicity. Overall, the P atoms bring evident electron redistribution, and the variation of chemical bonding is expected to lead to preferable band structures as efficient light absorption materials.

In the previous analysis of the electronic properties, it has been predicted that P-doped *h*-BNNSs have good visible-light absorption characteristics. The absorption coefficient is evaluated according to the following expression:

$$\alpha(E) = \frac{4\pi e}{hc}\left[\frac{(\varepsilon_1^2+\varepsilon_2^2)^{1/2}-\varepsilon_1}{2}\right]^{1/2}, \qquad (2)$$

where the ε_1 and ε_2 are the real and imaginary parts of the frequency-dependent dielectric function, where

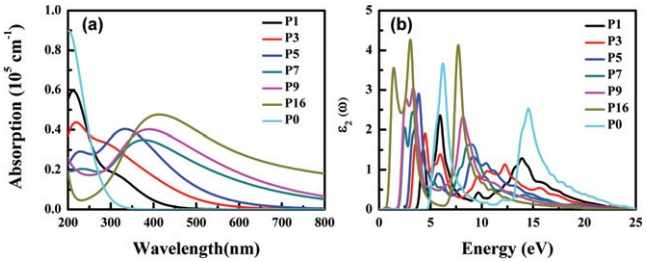

Fig. 7: The calculated absorption spectra and imaginary part ε_2 (ω) of the dielectric function for P-doped h-BNNSs compared to the pristine h-BN.

the imaginary part $\varepsilon_2(\omega)$ of the frequency-dependent dielectrics function can be expressed as follows:

$$\varepsilon^{(2)}_{\alpha\beta}(\omega) = \frac{4\pi^2 e^2}{\Omega} \lim_{q\to 0} \frac{1}{q^2} \sum_{c,v,k} 2\omega_k \delta(E_{ck} - E_{vk} - \omega) \times \langle \mu_{ck+e_\alpha q} | \mu_{vk} \rangle \left\langle \mu_{ck+e_\beta q} | \mu_{vk} \right\rangle^*, \quad (3)$$

where c and v refer to conduction and valence band states, respectively, and μ_{ck} refers to the cell periodic part of the wave functions at the k-point k. The real part of the dielectric function $\varepsilon^{(1)}_{\alpha\beta}(\omega)$ is derived from $\varepsilon^{(2)}_{\alpha\beta}(\omega)$ by a Kramers-Kronig transform. The results of the absorption spectrum are shown in fig. 7. The absorption spectrum for pristine h-BN (marked with P0 in fig. 7) is also illustrated for comparison. The absorption edge of h-BN locates at 350 nm. Compared with h-BN, all the P doping induces great red-shifts and extends the absorption edge to the visible-light region. Particularly, there are three evident and wide absorption peaks for P7-doped h-BNNSs, P9-doped h-BNNSs and P16-doped h-BPNSs at 380 nm, 390 nm and 410 nm, respectively, showing a good response to the visible-light irradiation. In addition, these three systems have shifted the absorption spectra from UV to the overall visible-light region. This phenomenon is related to the gradual narrowing of the band gap width of the P-doped h-BNNSs. Further insights into the optical transition can be explored by the imaginary part $\varepsilon_2(\omega)$ of the dielectric function (fig. 7(b)). In the case of pure h-BN, it has a smaller transition threshold compared to the band gap of 4.64 eV. Two distinct peaks are located at the high-energy region of 6 and 14 eV, which mainly come from band-band transition from N $2p$ in VBs to B $2p$ at CBs. When the P atoms are doped, these two intrinsic peaks both move to the lower-energy region. Moreover, one remarkable point is that an evident peak appears between 0 and 3.2 eV for P7-doped h-BNNSs, P9-doped h-BNNSs and P16-doped h-BPNSs, which corresponds to the band gap transition. This makes electron transition much easier and enhances the visible-light absorption in the low-energy region.

Through the analysis of band structure, PDOS and absorption spectrum, all P-doped h-BNNSs have an active response to the visible light. The enhanced mechanism of visible light can be described as follows: a) For P1 to P3-doped h-BNNSs with a relative larger band gaps, the visible-light response could be ascribed to the appearance of IB even across the Fermi level. Therefore, it is easier for electrons to enter the excited state. b) For P5-P16 doping, the significantly improved absorption ability is due to the largely narrowed band gaps. Overall, P doping can largely modify the electronic and optical properties of h-BNNSs, which can expand the application of h-BN in nano-semiconductor and nano-photocatalyst devices. Finally, through a comparative analysis of the structural stability and absorption spectrum of the P-doped systems, it is concluded that the P7 and P9-doped h-BNNSs not only have good structural stability, but also have the strongest visible-light response, which has important application possibilities for h-BNNSs in visible nano-optical devices.

Conclusions. – In conclusion, a series of P-doped h-BNNSs were investigated to explore the doping effects in improving the electronic and optic properties of h-BNNSs by using first-principles calculations. The introduction of P atoms can reduce the width of the band gaps of h-BNNSs which is in the range from 4.643 eV to 0.824 eV. As a result, the conversion of h-BN from insulator to semiconductor is realized. This narrowest band gap makes the electron transition easier, which is also evidenced from the large distortion of chemical bonding in the hexatomic ring. All P doped h-BNNSs have an active response to the visible-light. One enhanced mechanism of visible light is proposed. To sum up, P-doped h-BNNSs show better electronic and optic properties, which are regarded as potential 2D semiconductor materials and visible-light active photocatalysts.

* * *

This work was supported by the Foundation of Lanzhou Institute of Chemical Physics, the National Natural Science Foundation of China (grant Nos. 51875550, 51872166), the Key Research and Development Program of Shandong Province, China (grant Nos. 2019GGX102064, 2019JZZY010313), and the Fundamental Research Fund for Shandong University, China (grant No. 2017JC032).

REFERENCES

[1] Rubio A., Corkill J. L. and Cohen M. L., *Phys. Rev. B*, **49** (1994) 5081.
[2] Li L. H., Cervenka J., Watanabe K., Taniguchi T. and Chen Y., *ACS Nano*, **8** (2014) 1457.
[3] Yu Y., Chen H., Liu Y., Craig V. S. J., Wang C., Li L. H. and Chen Y., *Adv. Mater. Interfaces*, **2** (2015) 1400267.
[4] An L., Yu Y., Bai C., Bai Y., Zhang B., Gao K., Wang X., Lai Z. and Zhang J., *npj 2D Mater. Appl.*, **3** (2019) 28.

[5] Bai Y., Zhang J., Wang Y., Cao Z., An L., Zhang B., Yu Y., Zhang J. and Wang C., *ACS Appl. Nano Mater.*, **2** (2019) 3187.
[6] Li L. H., Xing T., Chen Y. and Jones R., *Adv. Mater. Interfaces*, **1** (2014) 1300132.
[7] Liu J., Kutty R. G., Zheng Q., Eswariah V., Sreejith S. and Liu Z., *Small*, **13** (2017) 1602456.
[8] Vel L., Demazeau G. and Etourneau J., *Mater. Sci. Eng. B*, **10** (1991) 149.
[9] Zhou J., Wang Q., Sun Q. and Jena P., *Phys. Rev. B*, **81** (2010) 085442.
[10] Zhang Z., Zeng X. C. and Guo W., *J. Am. Chem. Soc.*, **133** (2011) 14831.
[11] Bhattacharya A., Bhattacharya S. and Das G. P., *Phys. Rev. B*, **85** (2012) 035415.
[12] Li X., Zhao J. and Yang J., *Sci. Rep.*, **3** (2013) 1858.
[13] Lu R., Li F., Salafranca J., Kan E., Xiao C. and Deng K., *Phys. Chem. Chem. Phys.,* **16** (2014) 4299.
[14] Weng Q., Kvashnin D. G., Wang X., Cretu O., Yang Y., Zhou M., Zhang C., Tang D. M., Sorokin P. B., Bando Y. and Golberg D., *Adv. Mater.*, **29** (2017) 1700695.
[15] Lu Q., Zhao Q., Yang T., Zhai C., Wang D. and Zhang M., *ACS Appl. Mater. Interfaces*, **10** (2018) 12947.
[16] Tang C., Bando Y., Huang Y., Yue S., Gu C., Xu F. and Golberg D., *J. Am. Chem. Soc.,* **127** (2005) 6552.
[17] Qian Q., Lei J., Wei J., Zhang Z., Tang G., Zhong K., Zheng Z. and Chen K. J., *npj 2D Mater. Appl.*, **3** (2019) 24.
[18] Kou L., Du A., Chen C. and Frauenheim T., *Nanoscale*, **6** (2014) 5156.
[19] Si H., Lian G., Wang A., Cui D., Zhao M., Wang Q. and Wong C. P., *Nano Lett.*, **15** (2015) 8122.
[20] Radhakrishnan S., Das D., Samanta A., de Los Reyes C. A., Deng L., Alemany L. B., Weldeghiorghis T. K., Khabashesku V. N., Kochat V., Jin Z., Sudeep P. M., Marti A. A., Chu C. W., Roy A., Tiwary C. S., Singh A. K. and Ajayan P. M., *Sci. Adv.*, **3** (2017) e1700842.
[21] Zhang J., Zhang B., Yu Y. and Wang C.-M., *EPL*, **127** (2019) 67003.
[22] Wang F., Cao Y., Wei S. and Zhou Y., *J. Mol. Model.*, **23** (2017) 23.
[23] Clark S. J., Segall M. D., Pickard C. J., Hasnip P. J., Probert M. I. J., Refson K. and Payne M. C., *Z. Kristallogr. Cryst. Mater.*, **220** (2005) 567.
[24] McNellis E. R., Meyer J. and Reuter K., *Phys. Rev. B*, **80** (2009) 205414.
[25] Hamann D. R., Schlüter M. and Chiang C., *Phys. Rev. Lett.*, **43** (1979) 1494.
[26] Perdew J. P., Burke K. and Ernzerhof M., *Phys. Rev. Lett.*, **77** (1996) 3865.
[27] Grimme S., *J. Comput. Chem.*, **27** (2006) 1787.
[28] Chadi D. J., *Phys. Rev. B*, **16** (1977) 1746.
[29] Ataca C., Topsakal M., Aktürk E. and Ciraci S., *J. Phys. Chem. C*, **115** (2011) 16354.
[30] Kvashnin D. G., Sorokin P. B., Seifert G. and Chernozatonskii L. A., *Phys. Chem. Chem. Phys.*, **17** (2015) 28770.
[31] Zhang C. and Sun Q., *J. Phys. Chem. Lett.*, **7** (2016) 2664.
[32] Topsakal M., Aktürk E. and Ciraci S., *Phys. Rev. B*, **79** (2009) 115442.